Volume 27
Number 22
14 June 2025
Pages 6309-6678

Green Chemistry

Cutting-edge research for a greener sustainable future

rsc.li/greenchem

ISSN 1463-9262

ROYAL SOCIETY
OF **CHEMISTRY**

PAPER
Klaus Müller-Buschbaum *et al.*
Tellurium recovery from the thermoelectric materials bismuth telluride and antimony telluride by chemical vapour transport

25 YEARS
ANNIVERSARY

Green Chemistry

ROYAL SOCIETY OF CHEMISTRY

PAPER

View Article Online
View Journal | View Issue

Check for updates

Cite this: *Green Chem.*, 2025, **27**, 6405

Tellurium recovery from the thermoelectric materials bismuth telluride and antimony telluride by chemical vapour transport†

Julian Burkhart,[a] Lucas H. Bemfert,[a] Eliane L. Mitura,[a] Moritz Maxeiner,[a] Ruben Maile,[a] Alexander E. Sedykh[a] and Klaus Müller-Buschbaum*[a,b]

This work investigates the recovery of elemental tellurium from the thermoelectric materials Bi_2Te_3 and Sb_2Te_3 *via* chemical vapour transport (CVT) using the abundant element sulfur. A one-step process is established, involving a redox reaction between the respective tellurides and sulfur, followed by transporting elemental tellurium with the transport agent sulfur at mild temperatures. Differential scanning calorimetry identifies the redox reaction process for both systems (Bi_2Te_3/S and Sb_2Te_3/S) to occur in the temperature range of 175–200 °C. Additionally, the reaction conditions were optimised, and recovery rates, as well as transport rates for closed and open experimental setups, were determined. A temperature gradient of 425 °C → 325 °C with a Te : S molar ratio of 1 : 1.25 is proposed as optimum for a closed experimental setup. For an open experimental setup, a temperature gradient of 500 °C → 300 °C allows establishing a way with short reaction time of 1 h, identifying it as the best experimental recycling setup. For the system Bi_2Te_3/S, these reaction conditions resulted in a recovery rate up to 76% h^{-1} (transport rate 151.2 mg h^{-1}) for the open experimental setup. Additionally, the possibility of instrumental upscaling was shown on a laboratory scale. In all cases, the purity of the recovered tellurium was analysed using PXRD, Raman spectroscopy, EDX and DTA/TG + MS. The purity of Te was increased to >99.9 wt% through a purification step of heating to 500 °C under an Ar atmosphere, surpassing the detection limit used.

Received 8th January 2025,
Accepted 21st March 2025

DOI: 10.1039/d5gc00108k

rsc.li/greenchem

Green foundation

1. Principles of green chemistry are used as the basis for a chemical recycling process of the toxic but critical resource Te: the use of non-toxic, less hazardous chemicals, low energy consumption and options for the re-use of reagents.
2. The chemical recycling process of tellurium from the thermoelectric materials Bi_2Te_3 and Sb_2Te_3 not only provides excellent separation of the components but also achieves this while incorporating beneficial principles of green chemistry: it utilizes a chemical vapour transport reaction with the abundant, non-toxic chemical sulphur, is carried out at medium temperatures, and allows sulphur to be reused in cycles.
3. Future research will focus on the implementation of a recovery step aiming at recovering the elements bismuth and antimony from Bi_2S_3 and Sb_2S_3, which are also considered as critical resources, and will also involve p- and n-type semiconductors including the element selenium.

Introduction

The demand for renewable energy sources has also significantly increased the demand for tellurium (Te) for the manufacturing of highly pure semiconductor materials, such as cadmium telluride (CdTe), used in thin-film solar cells.[1,2] Besides CdTe solar cells (≈40%), Te is widely used in other fields, such as thermoelectric materials (≈30%), as a metallurgical additive in various materials (≈15%), rubber manufacturing (≈5%), and other applications (≈10%).[3–5] However, the abundance of Te in the Earth's crust is only 1–5 ppb, which is even lower than that of gold or platinum, rendering Te a highly critical element.[4,6,7] Additionally, Te is mainly obtained as a by-product of copper mining, which involves hydrometallurgical processes, such as leaching (acidic or alkaline) and electrowinning, or pyrometallurgical processes, such as roasting, smelting and refining, leading to overall low Te recovery yields (30–40%).[2,4,7–9] Therefore, the market price of Te is

---

[a] *Institute of Inorganic and Analytical Chemistry, Justus-Liebig-University Giessen, Heinrich-Buff-Ring 17, 35392 Giessen, Germany. E-mail: kmbac@uni-giessen.de; https://www.uni-giessen.de/de/fbz/fb08/Inst/iaac/mueller-buschbaum*

[b] *Center for Materials Research (LAMA), Justus-Liebig-University Giessen, Heinrich-Buff-Ring 16, 35392 Giessen, Germany*

† Electronic supplementary information (ESI) available: Additional graphs and tables with recovery rates, transport rates and recovery yields of open and closed experimental setups. Thermal analysis investigations, results of PXRD, Raman spectroscopy, EDX spectroscopy and EDX elemental mappings for multiple samples. See DOI: https://doi.org/10.1039/d5gc00108k

highly vulnerable to fluctuations.[9,10] Another critical issue is the high Te import rate of countries without large Te deposits, such as countries of the European Union, which can lead to geopolitical supply risks.[11,12] In conclusion, the increased demand can result in a general prospective supply risk. Hence, a recovery process for Te-containing materials is necessary, preferably without using hazardous or toxic compounds and with a low energy requirement.

To the best of our knowledge, only a few recovery techniques are known for Te-containing secondary resources (solar cells or thermoelectric devices). These recovery techniques involve either hazardous chemicals, such as sulfuric acid or hydrogen peroxide, or complicated and high energy-consuming processes, such as multi-stage vacuum distillations.[4,12–16] Additionally, electrochemical approaches have been reported for the recycling of Te-based solar cells, potentially enabling a greener recovery of Te.[17] Altogether, further research is needed in this field, and in addition, these methods have not yet been investigated for Te-based thermoelectric devices.

Recently, Bemfert, Müller-Buschbaum *et al.* developed a chemical vapour transport (CVT) method to recover Te from CdTe using sulfur.[18,19] CVT reactions are well known for yielding single crystals in fundamental research but are also used in common industrial applications such as purification, *e.g.*, the van Arkel and de Boer, and Mond processes.[20] CVT reactions can be performed in open and closed experimental setups. In Fig. 1, a schematic of a closed (A) and an open (B) experimental setup is shown. In both setups, the transport agent (TA) reacts with the source material (SM) to form the transport species (TS). A different temperature at the sink shifts the reaction equilibrium, promoting back reaction and deposition of the purified compound (PC). In a closed system, a chemical equilibrium is reached, while in an open system, equilibrium is not achieved, allowing for higher transport rates and faster recovery.

In this work, the concept of transporting the element Te with sulfur (S), which was published by Binnewies in 1976, was used.[21] Binnewies showed that gaseous species TeS_x or Te_2S_y (x = 1–7, y = 1–6) are formed from the elements, as observed by mass spectrometry, and proposed a temperature gradient of 375 °C → 325 °C for a closed experimental setup.[21] The presence of these gaseous species was also calculated later.[22] The above-mentioned approach by Bemfert, Müller-Buschbaum *et al.* for the CdTe/S system showed that transport of Te with sulfur in a temperature gradient is possible from compounds such as tellurides due to a redox reaction of CdTe with sulfur and can be carried out in both closed and open experimental setups.[19] A tellurium recovery of 97.8% was achieved. Additionally, the purity of the recovered tellurium was determined as 99.1 wt% without further purification, with

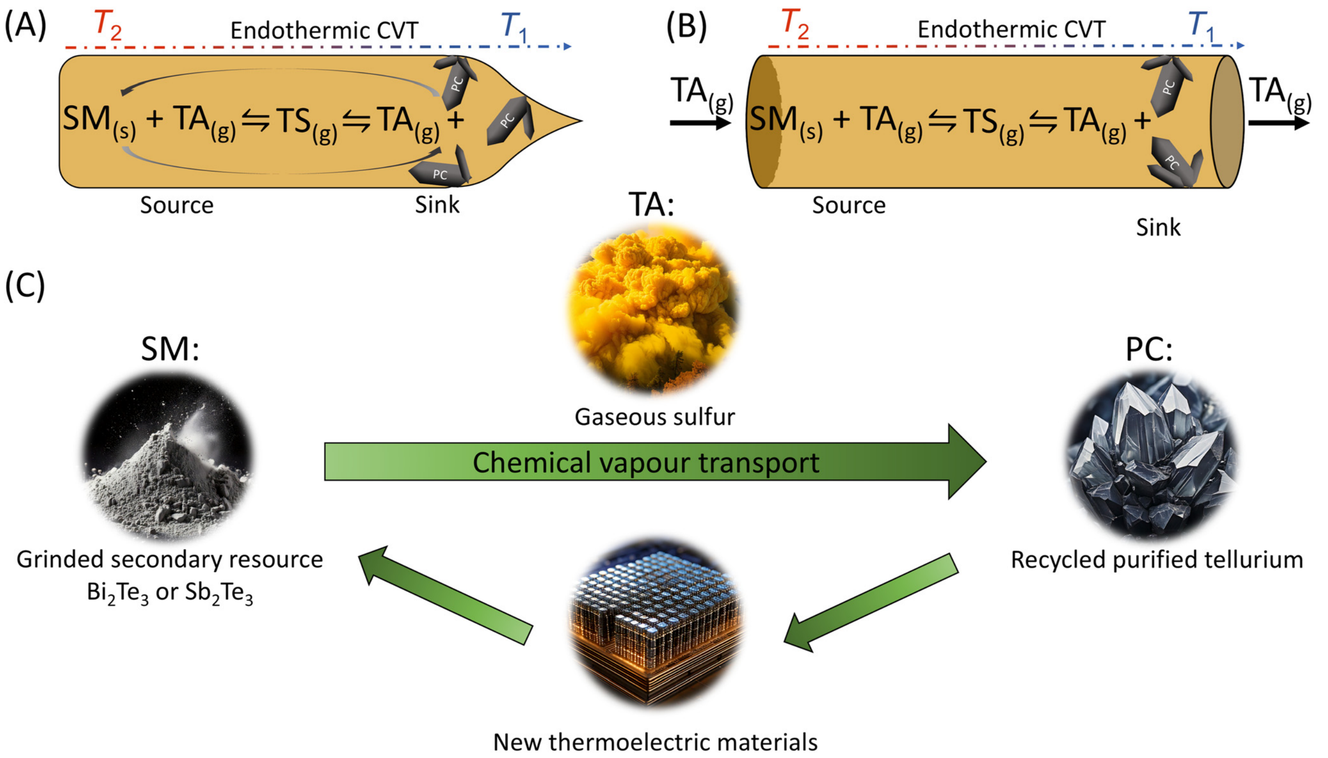
(A)
T_2
Endothermic CVT
T_1
$SM_{(s)} + TA_{(g)} \leftrightharpoons TS_{(g)} \leftrightharpoons TA_{(g)} +$
PC
PC
PC
Source
Sink
(B)
T_2
Endothermic CVT
T_1
$TA_{(g)}$
$SM_{(s)} + TA_{(g)} \leftrightharpoons TS_{(g)} \leftrightharpoons TA_{(g)} +$
$TA_{(g)}$
PC
PC
Source
Sink
TA:
(C)
Gaseous sulfur
SM:
PC:
Chemical vapour transport
Grinded secondary resource
Bi_2Te_3 or Sb_2Te_3
Recycled purified tellurium
New thermoelectric materials

Fig. 1 Schematic illustration of chemical vapour transport (CVT) in (A) a closed experimental setup and (B) an open experimental setup and (C) how this CVT can be part of a sustainable life cycle of Sb_2Te_3 and Bi_2Te_3. For an endothermic CVT reaction, as for both tellurides, the source material (SM) reacts with the transport agent (TA, here: S) at the higher temperature T_2 to form the transport species (TS). The transport species diffuses along a temperature gradient. At the lower temperature T_1, the back reaction takes place, and the original source material deposits in purified form at the sink (here: Te). This picture was partly created with AI (engine: Firefly).

sulfur being the only detectable impurity. In conclusion, compared to known processes, a recovery method with a lower energy requirement than the literature processes and without hazardous chemicals was developed.[19]

As mentioned above, thermoelectric materials make up about 30% of the overall use of Te.[3–5] These thermoelectric materials are typically composed of bismuth telluride (Bi_2Te_3) or antimony telluride (Sb_2Te_3) and are used as p-type compositions $Sb_{2-x}Bi_xTe_3$ or n-type compositions $Bi_2Te_{3-x}Se_x$ in thermoelectric devices.[23] Bi and Sb have also been described to be suitable for CVT reactions together with halogens as the TA, mostly iodine.[24] Accordingly, Bi and Sb could also be recovered by a subsequent CVT process. To the best of our knowledge, there are no CVT reactions with sulfur reported for these elements and their compounds, which would prevent separation of tellurium from these compounds. In general, using end-of-life thermoelectric materials as secondary resources can improve the Te supply in the future.[25] Therefore, this project aims to utilize CVT for the chemical recycling of tellurium from thermoelectric materials that is greener than established processes. Within this work, the binary systems Bi_2Te_3 and Sb_2Te_3 were investigated as model systems. Compared to the recycling techniques mentioned above,[4,12–16] this CVT approach offers, in accordance with the principles of green chemistry,[26] a greener method for recycling tellurium. The CVT approach requires less energy due to lower operating temperatures than multi-stage vacuum distillations and eliminates the need for hazardous chemicals used in solution-based methods. Furthermore, the TA sulfur can be reused multiple times to transport tellurium, minimizing waste and enhancing the overall sustainability of this CVT process.

Results and discussion

Characterization of the CVT recycling process of Te using thermal analysis

For the recovery of Te from Bi_2Te_3 and Sb_2Te_3, elemental sulfur was chosen as the transport agent. As shown for CdTe,[19] such an approach can form mixed tellurium–sulfur gas phase species directly from tellurides in addition to starting from the element Te.[21] CVT reactions can generally be performed in both closed and open experimental setups (see Fig. 1). A chemical equilibrium is only achievable in closed experimental setups, and the so-called transport agent (TA) can interact with the source material (SM) several times to form the so-called transport species (TS). Afterwards, the transport species, per definition, either diffuses from the higher temperature T_2 to the lower temperature T_1 in the case of an endothermic transport or *vice versa* for exothermic transport reactions. The different temperature at the sink shifts the equilibrium of the CVT reaction, which promotes the back reaction. Thus, the transported material is deposited at the sink as a purified compound (PC). In open experimental setups, the transport agent can interact with the source only once. Afterwards, depending on the CVT reaction, the transport agent either leaves the setup as a gas or deposits as a solid in colder regions beyond the sink temperature T_1. As a result, the transport agent has to be supplied continuously. Furthermore, the amount of transport agent added per time can highly influence the chemical equilibrium of the CVT reaction, which opens the possibility for higher transport rates, generally leading to faster recovery.

First, the relevant processes and parameters were identified. Here, differential scanning calorimetry (DSC) measurements were performed to investigate the redox reaction between the respective telluride and sulfur and the chemical vapour transport between tellurium and sulfur, as the method provides data on heat flow and relevant information on the temperature range and possible additional processes. For both tellurides, Bi_2Te_3 and Sb_2Te_3, two different mixtures of the respective telluride and sulfur were used, namely with molar ratios of Te : S of 1 : 2 and 1 : 1.25. Furthermore, reference measurements of sulfur, tellurium and the respective tellurides were carried out. During the heating process (Fig. 2A and 3A), the reference measurement of sulfur (green curve) shows three characteristic peaks for this element: the transition of orthorhombic α-sulfur to monoclinic β-sulfur (at 97 °C (1), lit.: 95–96 °C (ref. 27–29)); afterwards, melting of sulfur (at 113 °C (2), lit.: mp β-sulfur 119 °C (ref. 27–31)), with the determined onset value being in accordance with the published data; and the polymerisation of sulfur (at 161 °C (3), lit.: 159 °C (ref. 27, 29 and 31)). The melting point of sulfur (2) is also observable in all other investigations that include sulfur. In investigations of S together with both tellurides, peaks (1) and (3) are not observed due to the lower amounts of sulfur used in the mixtures. Additionally, during the heating process (Fig. 2A and 3A), the reference measurement of tellurium (blue curve) shows one characteristic peak, corresponding to its melting point at 449 °C ((4), lit.: mp Te 450 °C (ref. 32 and 33)). The reference measurement of bismuth telluride (orange curve) shows no signals in the measured temperature range, as expected. The reference measurement of antimony telluride should also show no signal in the measured temperature range. However, a peak (5) at 418 °C (see Fig. 3A) was observed in different purchased antimony tellurides. The antimony and tellurium phase diagram shows a eutectic temperature line at 422 °C (ref. 34), fitting with the observed signal and indicating an amount of elemental tellurium in the purchased compounds. Additionally, during the cooling process (see Fig. 2B and 3B), the reference investigation of sulfur shows a crystallisation signal at 69 °C (6). In the reference measurement of tellurium, the crystallisation signal is observable at 354 °C (7). Additionally, a crystallisation signal of the eutectic mixture at 400 °C (8) is visible in the reference measurement of antimony telluride (Fig. 3B). An enlarged graphic of each reference measurement can be found in Fig. S3–S6 in the ESI.†

Specific thermal properties of the Bi_2Te_3/S system. In order to investigate the potential chemical vapour transport of Bi_2Te_3 with S, two different molar ratios of Te : S were used (black: 1 : 2, red: 1 : 1.25) both for thermal investigations and for chemical vapour transport experiments in closed experimental setups. For both mixtures investigated, during the first half of the DSC cycle (Fig. 2A, heating), an exothermic signal

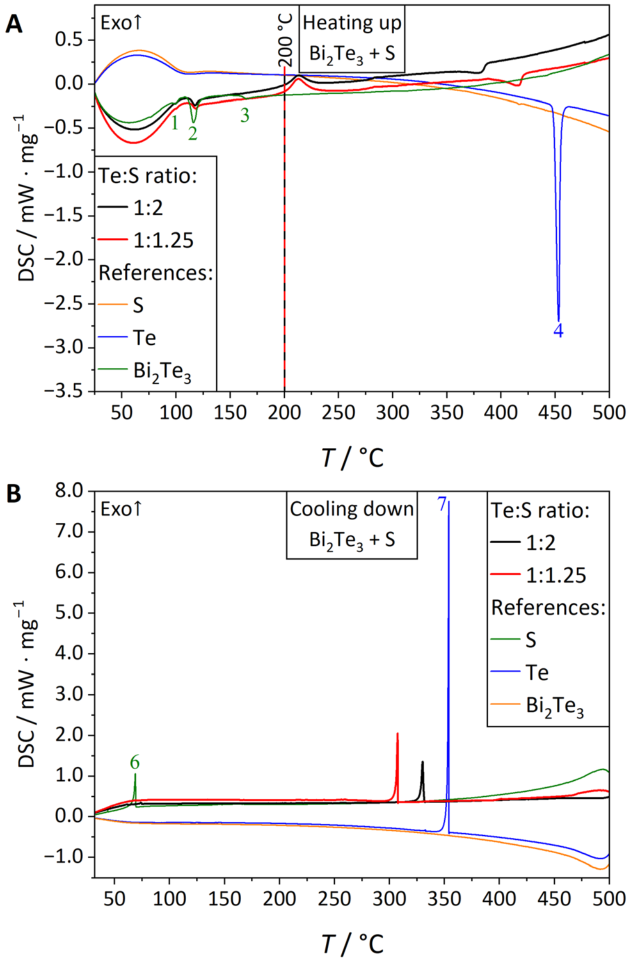

Fig. 2 DSC cycles (A: heating, B: cooling) of mixtures of bismuth telluride and sulfur for two different Te : S molar ratios (black: 1 : 2, red: 1 : 1.25) and for sulfur (green), tellurium (blue) and bismuth telluride (orange) as references. Additionally, in (A), the onset value of the redox reaction is marked with red and black lines.

appears at 200 °C. This peak corresponds to the exothermic redox reaction between bismuth telluride and sulfur (Scheme 1). This signal does not occur during the second measurement cycle (see Fig. S8†), confirming its assignment as a redox reaction signal according to Scheme 1.

The respective reaction was investigated for the first time in a closed experimental setup. To the best of our knowledge, there is only one other thermal analysis investigation of this reaction in the literature.[16] This measurement was performed in an open experimental setup under an argon atmosphere in a crucible that was not further described.[16] Ma *et al.* described three reactions between S and Bi_2Te_3 in a temperature range of 218–347 °C, which was determined by measuring the peak maximum.[16] The first signal's peak maximum at 218 °C aligns with the value determined in this work. The slight differences may originate from the different measurement conditions. In this work's closed DSC measurement (Fig. 2A), a second signal (360 °C and 390 °C, respectively) is observed, shifting towards the tellurium melting point (4) with decreasing sulfur content.

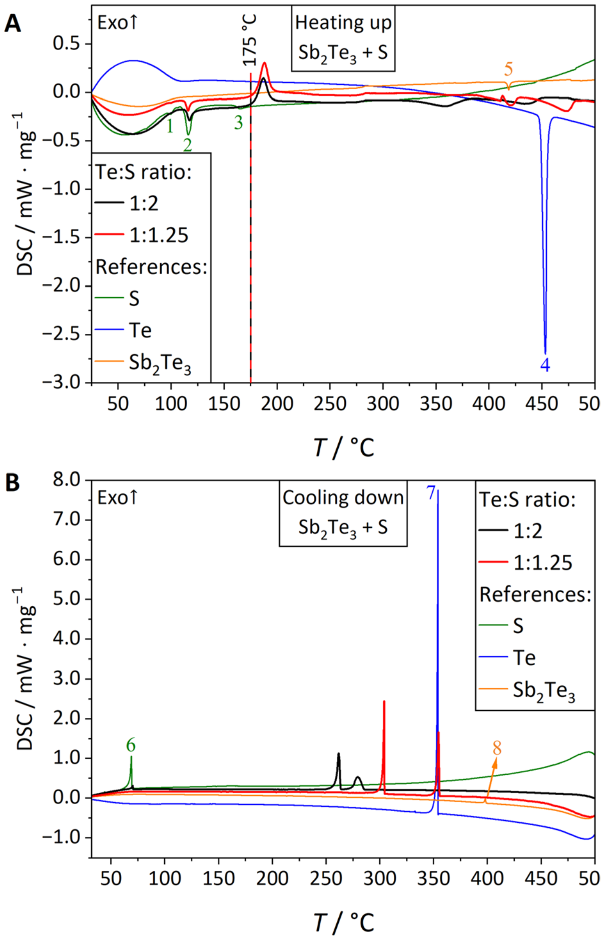

Fig. 3 DSC cycles (A: heating, B: cooling) of mixtures of antimony telluride and sulfur for two different Te : S molar ratios (black: 1 : 2, red: 1 : 1.25) and for sulfur (green), tellurium (blue) and antimony telluride (orange) as references. Additionally, in (A), the onset value of the redox reaction is marked with red and black lines.

$$Bi_2Te_3 + 3\,S \longrightarrow Bi_2S_3 + 3\,Te$$

Scheme 1 Exothermic redox reaction of bismuth telluride with sulfur.

This peak does not correspond to the endothermic transport reaction depicted in Scheme 2. Instead, a melting point depression of tellurium due to sulfur is proposed. A similar observation was reported for the CdTe/S system.[19] Therefore, the endothermic transport reaction (Scheme 2) is not visible for the Bi_2Te_3/S system.

During the second half of the DSC cycle (Fig. 2B, cooling), a crystallisation signal is observable for both molar ratios, located at 310 °C (1 : 1.25) or 330 °C (1 : 2). This signal corres-

$$y\,Te + S_x \xrightleftharpoons{\Delta T} S_{x\text{-}y}Te_y$$

Scheme 2 Endothermic transport reaction between tellurium and sulfur.

ponds to the crystallisation of the above-described sulfur–tellurium melt. Additionally, the measurement with a Te : S molar ratio of 1 : 2 shows a crystallisation peak at 73 °C corresponding to pure sulfur's crystallisation signal (6). An enlarged depiction of the shown DSC cycles of the different mixtures can be found in Fig. S7 in the ESI.†

Specific thermal properties of the Sb_2Te_3/S system. Also, for the Sb_2Te_3/S system, the two different molar ratios of tellurium to sulfur (black: 1 : 2, red: 1 : 1.25) were investigated. During the first half of the DSC cycle (Fig. 3A, heating), an exothermic signal occurs with an onset value of 175 °C. Again, it only appears during the first measurement cycle (see Fig. S10†) and is assumed to correspond to the redox reaction depicted in Scheme 3.

To the best of our knowledge, this reaction has been investigated with DSC for the first time, providing the respective results.

In addition to this exothermic redox signal, in both measurements (Fig. 3A, black and red curves), two endothermic signals appear in a temperature range of 325 °C to 500 °C. Again, they correspond to melting point depressions and shift towards the original melting points of tellurium and antimony sulfide with decreasing sulfur amounts. It is proposed that the first endothermic signal represents the melting point depression of tellurium, and the second originates from a melting point depression of antimony sulfide. Furthermore, during the second half of the investigations (Fig. 3B, cooling), two signals appear in the temperature range of 260 °C to 355 °C, also associated with the two melting point depressions, representing the crystallisation of the present melts. Additionally, the measurement with a Te : S molar ratio of 1 : 2 shows a crystallisation signal at 71 °C, corresponding to pure sulfur's crystallisation signal (6).

For the Bi_2Te_3/S system, the second endothermic melting signal (Fig. 3A) and the first crystallisation signal (Fig. 3B) are not present, as they are outside the investigated temperature range due to the higher melting point of bismuth sulfide (775 °C)[35] in comparison with antimony sulfide (546 °C).[36] The melting point depression of antimony sulfide was confirmed by DSC measurements of antimony sulfide and sulfur mixtures with two Sb_2S_3 : S molar ratios (1 : 1.5 and 1 : 3) according to the redox reaction shown in Scheme 3 (see Fig. S11†). In Fig. 3A, this melting point depression is assumed to be the second endothermic signal and is shifted to even lower values, indicating that the present tellurium also influences the melting point of antimony sulfide.

In general, due to the number of processes observed (chemical and physical), a complete clarification of all signals was not possible within this work. An enlarged depiction of the shown DSC cycles of the different mixtures can be found in Fig. S9 in the ESI.†

$$Sb_2Te_3 + 3\,S \longrightarrow Sb_2S_3 + 3\,Te$$

Scheme 3 Exothermic redox reaction of antimony telluride with sulfur.

CVT in closed experimental setups

To investigate the temperature dependence of the chemical vapour transport equilibria for the Bi_2Te_3/S and Sb_2Te_3/S systems, based on the results from DSC and the literature, eight different temperature gradients were selected in the range of 300–425 °C, and three ampoule reactions were prepared for each gradient. In the literature, a temperature gradient of 375 °C → 325 °C was used for the CVT of pure tellurium with sulfur, using a sulfur pressure of 0.05–0.3 bar (400 °C, calculated for S_4 and S_8) and a reaction time of 24 h, resulting in transport rates of 6.1–7.5 mg h^{-1} (0.61–0.75% h^{-1}).[21] In the case of the CdTe/S system, a slightly higher temperature of 400/425 °C at the source was reported as optimum to reach a recovery of Te of approximately 97% (≈1.4% h^{-1}/4 mg h^{-1}) after 72 h, using a sulfur pressure of 0.5–1 bar (400 °C, calculated for S_4 and S_8). Furthermore, it was suggested that a temperature gradient of 400 °C → 300 °C could be used for energy-saving purposes.[19]

In order to investigate the temperature dependence of the CVT, 150 mg of sulfur was used to guarantee a suitable pressure for CVT between approximately 0.5 and 1 bar (400 °C, calculated for S_4 and S_8). In Fig. 4, the resulting recovery yield (in %) of Te is shown as a function of sink and source temperatures. This recovery yield was calculated using the following eqn (E1):

$$\text{Recovery yield} = \frac{m(\text{Te}_{\text{Sink}})}{m(\text{Te}_{\text{Theoretical}})} \cdot 100\% \qquad \text{(E1)}$$

Fig. S1 in the ESI† shows a box diagram for both telluride systems with the exact values for each ampoule. In addition, the transport rate and recovery rate were calculated using the following eqn (E2) and (E3):

$$\text{Transport rate} = \frac{m(\text{Te}_{\text{Sink}})}{\text{Reaction time}} \qquad \text{(E2)}$$

$$\text{Recovery rate} = \frac{\text{Recovery yield}}{\text{Reaction time}} \qquad \text{(E3)}$$

Generally, for both systems Bi_2Te_3/S and Sb_2Te_3/S, higher temperatures at the source are favourable compared to published data.[21] For both systems, a nearly complete recovery (Bi_2Te_3/S: 99.8%, Sb_2Te_3/S: 97.7%) of Te was achieved for a temperature gradient of 425 °C → 325 °C, resulting in a recovery rate of approximately 1.4% h^{-1} and a transport rate of 4 mg h^{-1}. Furthermore, an energy-saving principle as for the system CdTe/S[19] can also be applied to Bi_2Te_3/S and Sb_2Te_3/S since Te recovery above 90% is still achievable with slightly lower temperature values of 400 °C → 300 °C. In general, it was possible to achieve higher recovery yields at the same temperature gradient for the Bi_2Te_3/S system than for the Sb_2Te_3/S system.

Besides the absolute temperatures at the source and sink, another significant value is the temperature difference ΔT between the source and sink. Fig. 5 shows the dependence of the Te recovery rate on ΔT. In general, it is observed that with increasing ΔT, the recovery rates increase. In agreement with thermodynamics, a small ΔT does not significantly influence the equilibrium of the CVT reaction (Scheme 2), and therefore, the transport rates are low. In contrast, higher ΔT shifts the equilibrium of the endothermic CVT reaction (Scheme 2) towards the transportation of Te and provides proper separation inside the ampoule. The maximum ΔT of 100 °C cannot be increased further for several reasons. First, due to the melting point of Te at approx. 450 °C,[33] at temperatures above 425 °C, slowly starts to sublime under reduced pressure and liquid Te would be able to distribute in the setup, both removing the separation of source and sink. Therefore, the maximum temperature at the source is fixed at 425 °C in a closed experimental setup with an applied pressure of 0.001 mbar. Second, due to the crystallisation temperature (325 ± 25 °C) of transported Te, temperatures below 300 °C would not improve the CVT. Instead, the source and sink would also be less separated. Therefore, it is suggested to set ΔT in a range of 75–100 °C to guarantee a change in CVT equilibrium and a proper separation.

As described in the beginning of this section, in the literature, different pressure ranges of 0.05–0.3 bar (ref. 21) and 0.5–1 bar (ref. 19) (400 °C, calculated for S_4 and S_8) and different reaction times of 24 h (ref. 21) and 72 h (ref. 19) have been reported. Thus, the Te : S molar ratio and the reaction time were investigated to identify the best reaction properties for the Bi_2Te_3/S system.

In Fig. 6, two molar ratios of Te : S (1 : 2 and 1 : 1.25) and three reaction times (24, 48, 72 h) are shown for two temperature gradients (red: 375 °C → 325 °C, grey: 425 °C → 325 °C).

By comparison of the recovery rates at the two different temperature gradients, it can be seen that for the 375 °C → 325 °C gradient (red boxes), the CVT is not finished after 72 h and is independent of the Te : S molar ratio and reaction time. At the temperature gradient of 425 °C → 325 °C, the recovery rate decreases with increasing reaction time, due to the higher amount of transported tellurium, which influences the chemical equilibrium of the CVT. This behaviour is in accordance with the general principle of closed CVT reactions. A more detailed investigation of how the recovery rates develop over

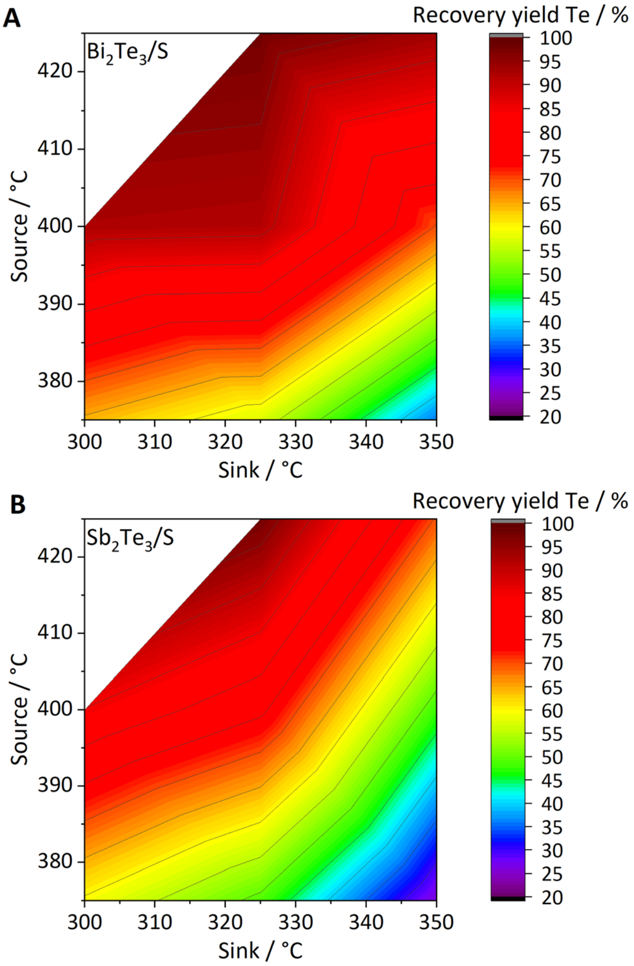

Fig. 4 Heat maps of different temperatures at the source and sink in combination with the recovery yield of Te for (A) Bi_2Te_3/S and (B) Sb_2Te_3/S.

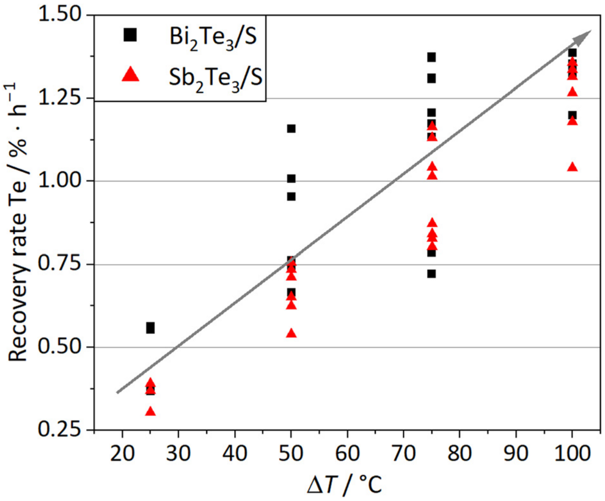

Fig. 5 Recovery rate of Te in relation to the temperature difference ΔT between the source and sink for the Bi_2Te_3/S (black squares) and Sb_2Te_3/S (red triangles) systems.

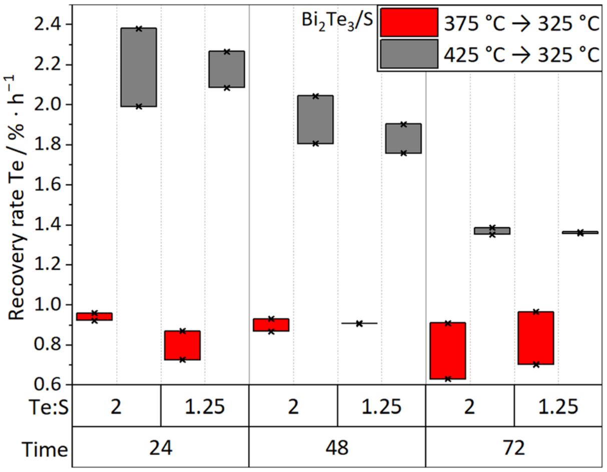

Fig. 6 Recovery rates of Te for the Bi_2Te_3/S system in relation to two different Te : S molar ratios (1 : 2, 1 : 1.25) at two different temperature gradients (red boxes: 375 °C → 325 °C, grey boxes: 425 °C → 325 °C) and a reaction time of 24 h, 48 h or 72 h. The exact transport rates for each ampoule are marked with a black cross.

time (1 h, 2 h, 4 h, 8 h, 24 h, 48 h, 72 h) at a temperature gradient of 425 °C → 325 °C is shown in Fig. S2 in the ESI.† Both data (Fig. S2† and Fig. 6) show that the CVT is nearly finished after 48 h with a recovery yield of 98% ($\approx$2.0% h^{-1}/6.1 mg h^{-1}) in the best case. In general, the Te : S molar ratio does not influence the recovery rates significantly. Additionally, it should be noted that for the lower Te : S molar ratio of 1 : 1.25, sulfur deposition is more controllable, making it easier to get tellurium with higher purities, and therefore should be used for further investigations.

In summary, for the Bi_2Te_3/S system, it is proposed that further investigations of closed experimental setups should use a temperature gradient of 425 °C → 325 °C, a Te : S molar ratio of 1 : 1.25, and a reaction time of 48 h. These conditions (425 °C → 325 °C, Te : S 1 : 1.25, 48 h) were also tested for the Sb_2Te_3/S system and resulted in a recovery yield of 65.2% ($\approx$1.4% h^{-1}/4.1 mg h^{-1}). Since the recovery rates were always slightly lower for the Sb_2Te_3/S system, a reaction time longer than 48 h is needed for the complete transport of tellurium in closed experimental setups.

CVT in open experimental setups

CVT reactions in open experimental setups are more suitable for industrial applications compared to closed ones, mainly due to the possibility of creating a circulating gas flow setup. Therefore, the parameters gathered from investigations of the closed experimental setup mentioned above were used to develop an open experimental setup for both telluride systems under investigation. For the transport process, the most significant difference between open and closed experimental CVT setups is that in an open experimental setup, the used transport agent can only take part once in the transport reaction during its dwell time at the source and deposits after being moved by the gas flow at the end of the reaction tube. Furthermore, it is known from the literature that the used sulfur evaporates below the boiling point[27] at 444 °C.[16,19] Therefore, sulfur cannot be wholly used to transport tellurium in an open experimental setup. Hence, it is necessary to increase the excess of sulfur at the beginning of the recovery process. Furthermore, the supply of additional sulfur to the process should be possible after a defined reaction time, preferably by cycling of the used sulfur. Moreover, in open processes, the CVT reaction (Scheme 2) does not reach a chemical equilibrium like in a closed experimental setup. Due to the open character and the increased amount of sulfur, the CVT equilibrium is pushed towards the product site. This enables the possibility of higher transport and recovery rates, which is highly favourable for industrial applications at the cost of additional sulfur, if it is not re-used. Fig. 7 shows a schematic illustration of an open recovery process. In addition to the first amount of sulfur, which was mixed with the respective telluride at T_3, a second amount of sulfur was placed at T_4 to mimic the re-use of sulfur after transport. This sulfur amount could be heated after a defined reaction time. In a commercial process, this step can be substituted either with a circulating sulfur gas flow or with the recovery of the solid sulfur, which can then take part in the process several times. Generally, re-use should guarantee a low consumption of sulfur and reduce the loss of tellurium still incorporated in mixed rings with sulfur.

For both Bi_2Te_3/S and Sb_2Te_3/S systems, Table 1 presents parameters and recovery rates for different experimental conditions. At first, the same temperature gradient (425 °C → 325 °C) was chosen as in the best-performing closed experimental setup. At this temperature gradient (425 °C → 300 °C), a tellurium recovery rate of 24% h^{-1} (transport rate 48.5 mg h^{-1}) was achieved for the Bi_2Te_3/S system. Compared to the recovery rate of the best-performing closed experimental setup ($\approx$2% h^{-1}/transport rate 6.1 mg h^{-1}), this value is already ten times higher, showing that the recovery rates of open processes can be increased to a much greater extent.

Besides slightly higher temperatures of 500 °C → 300 °C for optimal open transport, the limiting factor for higher recovery rates is the amount of sulfur required. Therefore, to simulate the potential cycling of sulfur, a second amount of sulfur was located at T_4 being necessary to further increase the recovery rates. As a result, the recovery rate could be increased to a maximum value of 76% h^{-1} (transport rate 151.2 mg h^{-1}) for the Bi_2Te_3/S system. No tellurium could be detected with PXRD in the source material (see Fig. 8B), so it is assumed that nearly complete transportation occurred.

An increase in the argon flow also has an influence on the recovery rate. Increasing the flow from 0.15 NL h^{-1} cm^{-2} to 1.5

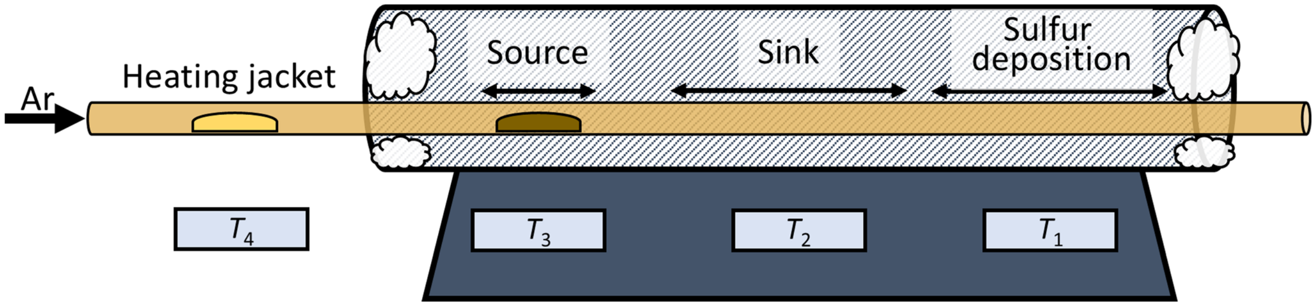

Fig. 7 Schematic illustration of an open experimental setup. At the source, the mixture of telluride and sulfur is shown in brown. Additionally, the second amount of sulfur is shown in yellow located at T_4.

Table 1 Parameters and recovery rates for the open Bi_2Te_3 and Sb_2Te_3 recovery processes

System	T_1/°C	T_2/°C	T_3/°C	T_4/°C	Te : S molar ratio	t /h	ν (Ar)/NL h^{-1} cm^{-2}	Recovery rate (Te) /% h^{-1}
Bi_2Te_3	300	325	425	—	1 : 30	1	0.15	24
Bi_2Te_3	300	350	500	—	1 : 30	1	0.15	39
Bi_2Te_3	300	350	500	500	1 : 60	1	0.15	76
Bi_2Te_3	300	350	500	500	1 : 60	1	1.5	62
Sb_2Te_3	300	325	425	—	1 : 30	1	0.15	18
Sb_2Te_3	300	350	500	—	1 : 30	1	0.15	36
Sb_2Te_3	300	350	500	500	1 : 60	1	0.15	61
Sb_2Te_3	300	350	500	500	1 : 60	1	1.5	43

NL h^{-1} cm^{-2} results in a reduced recovery rate of 62% h^{-1} (transport rate 123.1 mg h^{-1}) for the Bi_2Te_3/S system. A high stream of flow gas minimized the contact time of S with Bi_2Te_3 and Sb_2Te_3. Additionally, it may increase the amount of tellurium still incorporated in mixed rings and hamper the time for tellurium deposition after transport.

For the Sb_2Te_3/S system, the respective recovery rates show a similar trend (see Table 1). The same experimental setup (500 °C → 350 °C → 300 °C, 0.15 NL h^{-1} cm^{-2}) led to the best recovery rate of 61% h^{-1} (transport rate 121.1 mg h^{-1}). Also, the absolute recovery rates are slightly lower, as observed for the closed experimental setup.

In summary, a temperature gradient of 500 °C → 350 °C → 300 °C with an argon flow of 0.15 NL h^{-1} cm^{-2} was the best experimental setup for both investigated systems.

A comparison with the CdTe/S system (best open experimental setup: 5.6% h^{-1}/7.1 mg h^{-1})[19] shows that the recovery process for Bi_2Te_3 and Sb_2Te_3 is even more preferable, leading to higher rates in terms of recovery and transportation. The crucial changes in the experimental parameters in comparison with the experimental setup used for the CdTe/S[19] system were a reduction in the reaction time, an increase in the source temperature, and the use of a second amount of sulfur, which could be evaporated after a defined reaction time, thereby extending the CVT to simulate a continuous sulfur gas flow.

The possibility of upscaling the process was investigated by doubling the amount of reagents, increasing the tube diameter, and creating a deepening in the glass tube (depth: 1 cm, length: 2 cm) at the source and the location for the second sulfur supply to avoid floating of the melts. All other parameters were kept the same. PXRD data of the sink and source for both upscaled systems can be found in Fig. S19 in the ESI.† This upscaling yields recovery rates of 54% h^{-1} (transport rate 215.1 mg h^{-1}) for the Bi_2Te_3/S system and 44% h^{-1} (transport rate 175.8 mg h^{-1}) for the Sb_2Te_3/S system. Thus, upscaling of the process is possible. Additionally, due to the higher amount of sulfur, it was impossible to avoid a small back diffusion of the sulfur, leading to less sulfur participating in the process. By eliminating this drawback, the CVT process could be used to recover higher amounts of tellurium.

Purity analysis

Powder X-ray diffraction. The received products at the source and sink of both systems were investigated with PXRD to determine the purity of the recovered tellurium and the composition of the source residuals. In Fig. 8, the PXRD results of the best closed experimental setup (A) and the best open experimental setup (B) are shown for the Bi_2Te_3/S system. In both cases, the reactions were performed at the respective optimal temperature gradient (closed: 425 → 325 °C; open: 500 → 300 °C). In both closed and open experiments, the investigation of the sink material shows only tellurium reflections[37] without any reflections of sulfur,[38] indicating that the CVT recovery method led to tellurium with high purity. Depending on the tellurium recovery yield, the source shows only sulfide reflections[39] at high recovery yields, as shown in Fig. 8(A and B). Tellurium reflections are also visible at lower recovery yields (see Fig. S12–S20†). The same results were also observed for all other Bi_2Te_3/S investigations. For all closed and open Bi_2Te_3/S investigations, exemplary powder diffractograms of the source and sink are shown for each experimental setup in Fig. S12, S14–S16, and S19, in the ESI.†

In general, PXRD investigations for the closed and open Sb_2Te_3/S experimental setups show similar results, with the formation of Sb_2S_3 [40] instead of Bi_2S_3. Fig. S13, S17, S18, and S20 in the ESI† provide powder diffractograms for all closed and open Sb_2Te_3/S investigations.

In addition, the upscaling experiments also show corroborating results without crystalline impurities, as shown in Fig. 8C for the open Sb_2Te_3/S investigation.

Raman spectroscopy. Raman investigations of the recovered tellurium and pure sulfur as a reference were performed to further investigate the purity of the recovered tellurium. In general, Raman measurements can be used as a detection method for sulfur impurities since sharp sulfur modes were already visible at lower laser power in comparison with the tellurium modes. The spectra are shown in Fig. 9 for tellurium recovered in the respective best-performing closed (A) and open (B) experimental setups of the Sb_2Te_3/S system. Typical tellurium modes are observable in both cases, and no sulfur modes were detected. In general, one sulfur mode is present, which could overlap with the tellurium mode at 141 cm^{-1}. Since this sulfur mode does not exhibit the highest intensity, present sulfur impurities should still be observable using the missing sulfur mode at 220 cm^{-1}. This again indicates, like the PXRD measurements, that the CVT recovery method led to tellurium with no detectable sulfur impurities, assuming a high Te purity. Specific tellurium modes observed are E^1

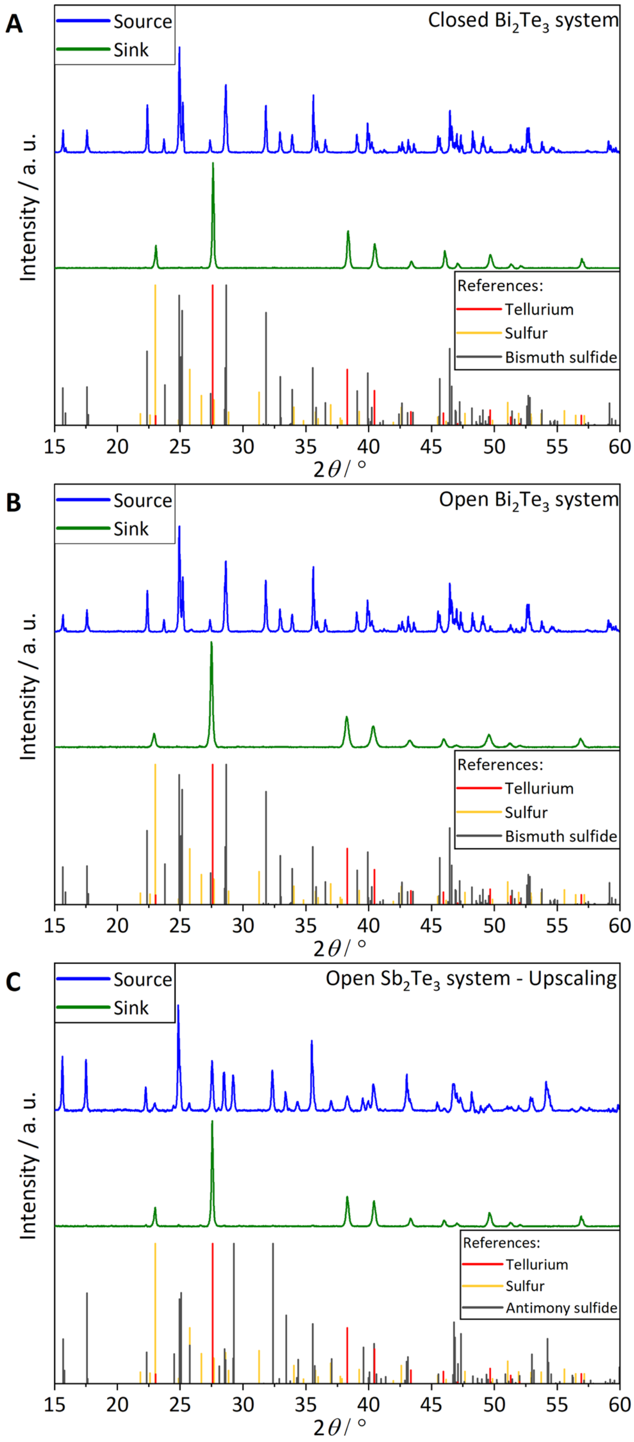

Fig. 8 PXRD data of the source (blue diffractogram) and sink (green diffractogram) products of (A) the best closed and (B) the best open Bi_2Te_3/S experimental setup and (C) the Sb_2Te_3/S upscaling setup. Additionally, references for tellurium,[33] sulfur,[34] bismuth sulfide[35] and antimony sulfide[36] are shown.

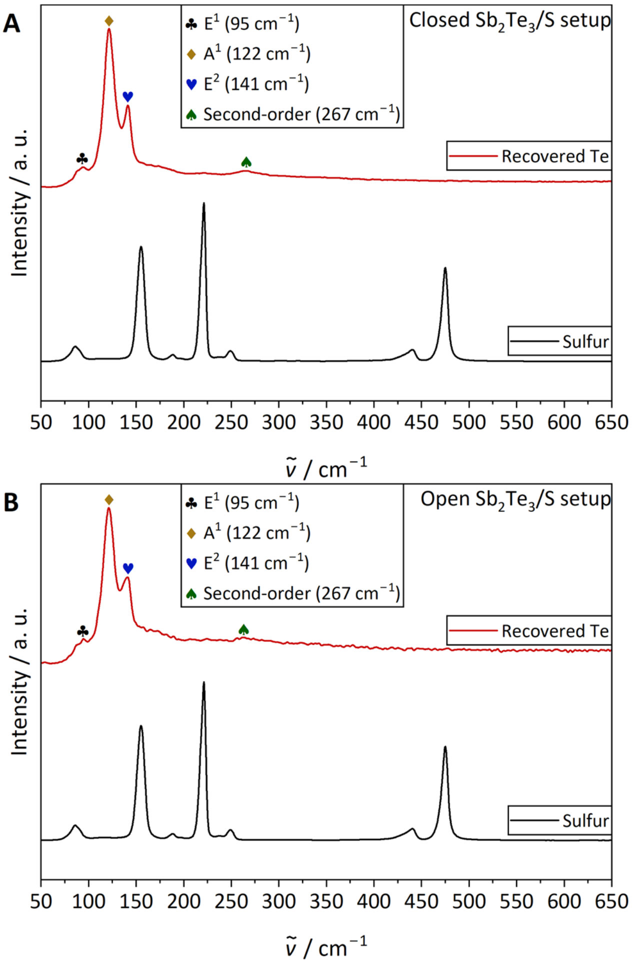

Fig. 9 Raman spectra of tellurium recovered in (A) the best closed and (B) the best open Sb_2Te_3/S experimental setup. A reference measurement of sulfur is also shown, and the specific Raman modes of tellurium are marked.

(95 cm^{-1}), A^1 (122 cm^{-1}), E^2 (141 cm^{-1}) and a second-order mode from the E mode (267 cm^{-1}). These values align well with the reported range in the literature.[41a–f,42] A^1 (122 cm^{-1}) corresponds to symmetric expansion and compression in the basal plane. E^1 (95 cm^{-1}) originates from chain rotation over the *a*- or *b*-axis, and E^2 (141 cm^{-1}) results from asymmetric stretching mostly occurring along the *c*-axis.[42,43]

Also, the Raman spectra for the respective best-performing Bi_2Te_3/S experimental setups show the same results and can be found in Fig. S21 in the ESI.† In summary, this measurement also shows no detectable sulfur impurities in the recovered tellurium.

Energy-dispersive X-ray analysis. In addition to the purity check by PXRD and Raman spectroscopy, the recovered tellurium was also investigated using energy-dispersive X-ray analysis (EDX). EDX is more sensitive in detecting smaller impurities than the other methods. Furthermore, it is possible to quantify the present elements, with limitations for elements with a high difference in molar mass. The results are presented in Fig. 10 for tellurium recovered in the best closed (A) and open (B) experimental setups for the Bi_2Te_3/S system. In both experimental setups and for both telluride systems (see Fig. S22 and S23†), tellurium purities >99 wt% could be

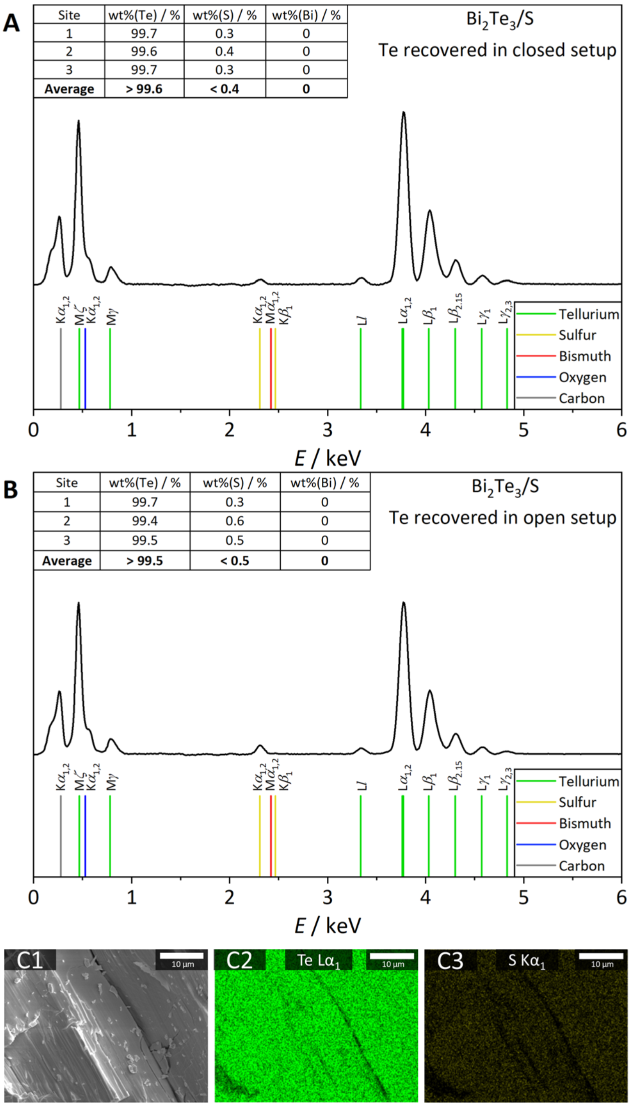

A

Site	wt%(Te) / %	wt%(S) / %	wt%(Bi) / %
1	99.7	0.3	0
2	99.6	0.4	0
3	99.7	0.3	0
Average	**> 99.6**	**< 0.4**	**0**

Bi_2Te_3/S
Te recovered in closed setup

B

Site	wt%(Te) / %	wt%(S) / %	wt%(Bi) / %
1	99.7	0.3	0
2	99.4	0.6	0
3	99.5	0.5	0
Average	**> 99.5**	**< 0.5**	**0**

Bi_2Te_3/S
Te recovered in open setup

Fig. 10 EDX data of tellurium recovered in (A) the best closed ampoule and (B) the best open experimental setup of the Bi_2Te_3/S system. For each sample, an average wt% value is given. It is calculated from three different measuring spots. Characteristic X-ray emission lines are also shown for tellurium, sulfur, bismuth, oxygen, and carbon as references.[40] Additionally, the surface (C1) of tellurium recovered in the best-performing closed ampoule of the Bi_2Te_3/S system and respective elemental mappings of tellurium (C2, green dots) and sulfur (C3, yellow dots) are shown.

achieved without a further purification step. Furthermore, the only visible impurities are sulfur residues. In a direct comparison between the tellurium recovered in closed and open experimental setups, the purities achieved in closed experimental setups are slightly higher. This trend is in accordance with the much slower process and the slower formation of tellurium crystals in a closed ampoule compared to an open experimental setup. Consistently, the amount of sulfur is higher in the open experimental setup than in the closed one, leading to slightly higher sulfur wt% values. Fig. 10C shows an SEM image of the surface of tellurium recovered in a closed

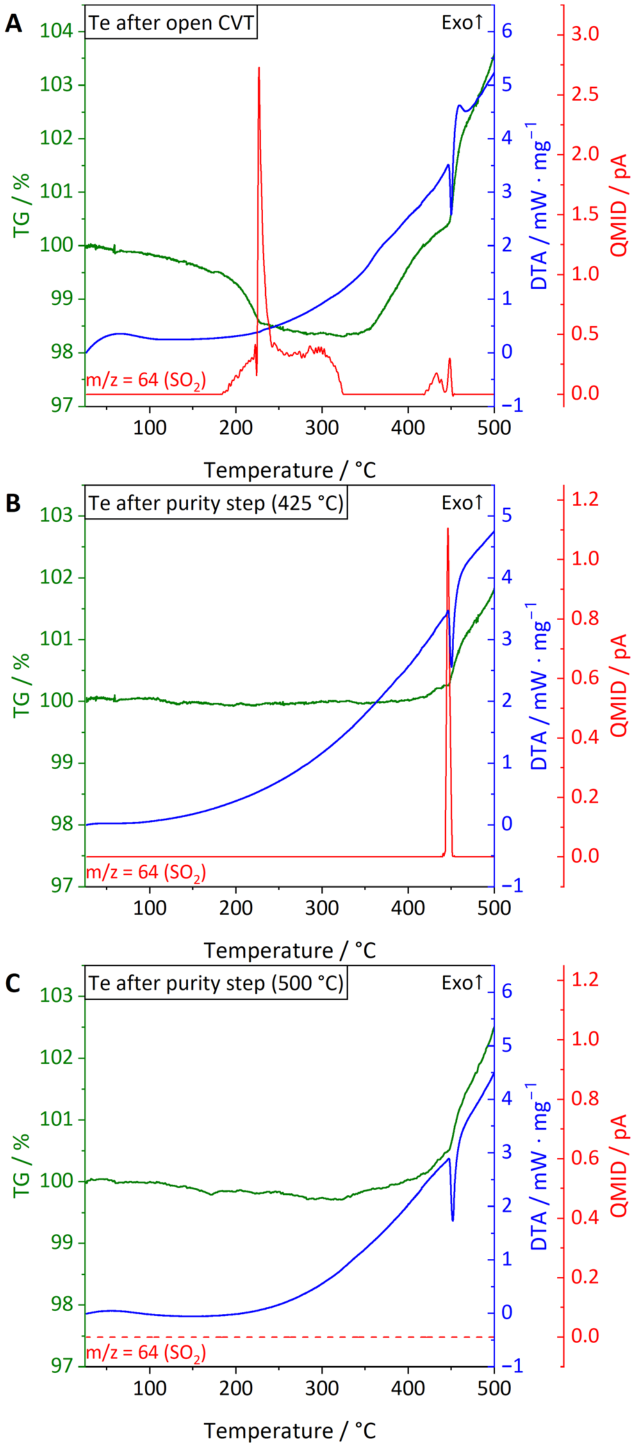

Fig. 11 STA investigations of three tellurium samples are shown. In each diagram, a TG curve (green), a DTA curve (blue), and a QMID curve (red) are shown. (A) shows the investigation of a tellurium sample recovered with the best open experimental setup. (B) shows the investigation of a tellurium sample recovered with the best open experimental setup, which was additionally heated to 425 °C as a purification step. (C) shows the investigation of a tellurium sample recovered with the best open experimental setup, which was additionally heated to 500 °C as a purification step.

ampoule (C1), an elemental mapping of tellurium (C2, green dots) and an elemental mapping of sulfur (C3, yellow dots). A homogeneous elemental distribution of tellurium and sulfur is present. This observation applies to all measured samples and can be seen in Fig. S24–S28 in the ESI.†

Purification step

Since the EDX results revealed small sulfur impurities, a purification step was developed to remove these residuals. A heating step of the recovered tellurium under an argon atmosphere was chosen for purification. Simultaneous thermal analysis (STA) under a synthetic air atmosphere was used to determine the temperature that is sufficient to completely evaporate sulfur residues in the recovered tellurium. During the process, sulfur residuals were oxidised to SO_2 (m/z = 64), which was detected with the coupled mass spectrometer. Furthermore, the thermogravimetric curve (TG) can be used to determine the amount of sulfur present in the sample after the CVT. Fig. 11 shows a comparison of three STA investigations of non-purified and purified tellurium samples recovered under the best conditions for open CVT. In Fig. 11A, two temperature ranges are visible in which SO_2 is formed during the process, indicating sulfur as an impurity, which are not present (11C) or only partly present (11B) in the purified samples: first, between 180 °C and 325 °C and second, at the tellurium melting point (450 °C). Furthermore, the TG curve shows a mass loss of approximately 1.7% during the first detection of SO_2 between 180 °C and 325 °C, resulting in slightly higher wt% after the CVT compared to the EDX measurement (0.3–1.6 wt%). Furthermore, it is assumed that sulfur that evaporates and oxidises between 180 °C and 325 °C is located at the surface of tellurium, and sulfur that evaporates and oxidises at the tellurium melting point is located inside the transported material. This assumption is confirmed by Fig. 11B and C, indicating that a temperature of 425 °C during the purification step is insufficient to evaporate all sulfur residues; here, only the sulfur located at the surface was removed (see Fig. 11B). An increase in temperature above the melting point of tellurium resulted in no SO_2 detection (see Fig. 11C). Hence, the sulfur residuals present after CVT are removed with the purification step at 500 °C.

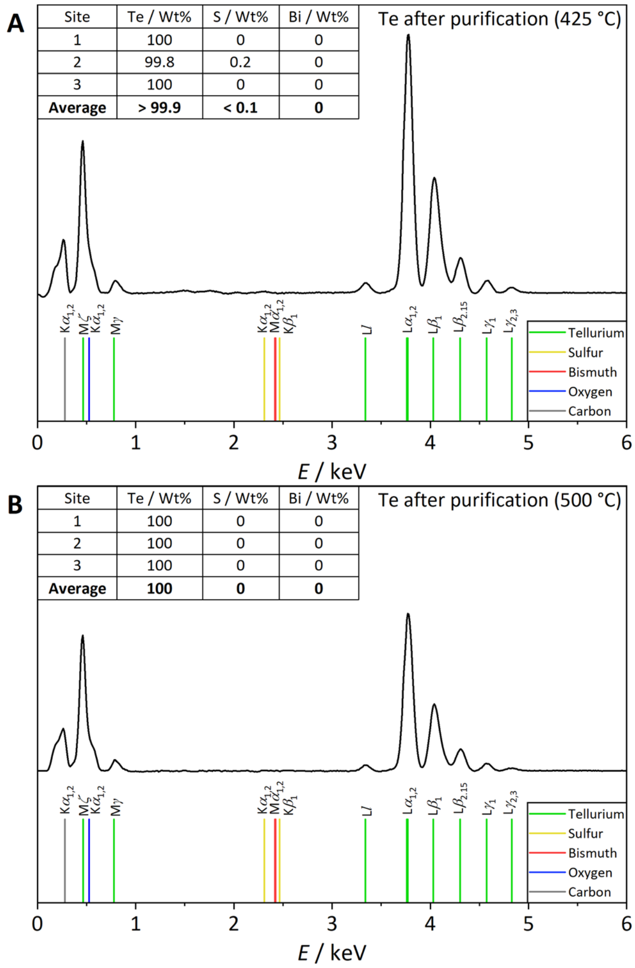

A

Site	Te / Wt%	S / Wt%	Bi / Wt%
1	100	0	0
2	99.8	0.2	0
3	100	0	0
Average	**> 99.9**	**< 0.1**	**0**

B

Site	Te / Wt%	S / Wt%	Bi / Wt%
1	100	0	0
2	100	0	0
3	100	0	0
Average	**100**	**0**	**0**

Fig. 12 EDX data of tellurium purified at (A) a temperature of 425 °C and (B) a temperature of 500 °C. For each element, an average wt% value is given. It is calculated from three different measuring spots. Characteristic X-ray emission lines are also shown for tellurium, sulfur, bismuth, oxygen, and carbon as references.[40]

Additionally, the purity of tellurium after the different purification steps was investigated using EDX. The results are shown in Fig. 12 for both purification temperatures. After the purification step at 425 °C (Fig. 12A), only trace amounts of sulfur residues (<0.1 wt%) were detected. After the purification step at 500 °C, no sulfur residues were detectable with this method (see Fig. S29 and S30†). Altogether, the purity of the recovered tellurium increased to >99.9 wt%, exceeding the detection limit of the EDX device.

Conclusions

In this work, a CVT-based recovery method was successfully established for the thermoelectric compounds Bi_2Te_3 and Sb_2Te_3 together with sulfur as a transport agent. The process yields better results than those achieved for the transport of CdTe with S. In comparison with the known processes for the recovery of Te, such as leaching or multi-vacuum distillation, the presented recovery method works without using hazardous and non-abundant chemicals, and consumes less energy due to a maximum temperature limit of 500 °C. At the beginning of the recovery process, the method uses sulfur as an oxidising agent, forming the respective sulfides and elemental tellurium at a temperature of only 200 °C (Bi_2Te_3/S) or 175 °C (Sb_2Te_3/S). Afterwards, an endothermic CVT reaction with sulfur occurs, whereby tellurium atoms are incorporated into the sulfur rings, forming the transport species (TeS_{1-7} or Te_2S_{1-6}) that separate tellurium from the source material. To the best of our knowledge, this is the first time this process has been described, starting with the thermoelectric material Bi_2Te_3 or Sb_2Te_3.

For the investigated closed experimental setup, the optimal conditions were a temperature gradient of 425 °C → 325 °C, a reaction time of 48 h and a Te : S molar ratio of 1 : 1.25 (Bi_2Te_3/S: 2.0% h^{-1}/6.1 mg h^{-1}, Sb_2Te_3/S: 1.4% h^{-1}/4.1 mg h^{-1}).

For the investigated open experimental setup, the optimal conditions were a temperature gradient of 500 °C → 350 °C → 300 °C, a reaction time of only 1 h and an argon flow of 0.15 NL h^{-1} cm^{-2} (Bi_2Te_3/S: 76% h^{-1}/151.2 mg h^{-1}, Sb_2Te_3/S: 61% h^{-1}/121.1 mg h^{-1}).

Furthermore, upscaling in a larger experimental setup and doubling the amount of reagents gave promising results for the Bi_2Te_3/S system (54% h^{-1}/215.1 mg h^{-1}) and the Sb_2Te_3/S system (44% h^{-1}/175.8 mg h^{-1}).

In general, the recovery rates and transport rates for the Sb_2Te_3/S system were consistently slightly lower but within the same range and with the same tendencies as those for the Bi_2Te_3/S system.

PXRD and Raman spectroscopy showed no impurities in the recovered tellurium. EDX detected only small sulfur residuals, resulting in a good Te purity above 99 wt% after this one-step recovery process with no further purification. A one-step heating to 500 °C under an argon atmosphere was established for purification of the recovered tellurium, removing sulfur impurities within our detection limits, resulting in a high Te purity of >99.9 wt%.

Additionally, a second recycling step to recover the critical elements bismuth and antimony would be highly beneficial, and a CVT-based process using halogens as TA could be coupled to the process described here for this purpose. However, the use of halogens is problematic from a green chemistry perspective.

While this study demonstrates the effectiveness of recycling tellurium starting from the binary phases Bi_2Te_3 and Sb_2Te_3, future research could expand to the recycling of ternary p- and n-type compositions used in thermoelectric devices that also contain selenium. Recycling of p-type $Sb_{2-x}Bi_xTe_3$ should proceed without significant issues, as it contains the same elements investigated here. For n-type $Bi_2Te_{3-x}Se_x$, the selenium content would be incorporated into the sulfur rings and transported *via* CVT as well, from which it is harder to separate than to separate tellurium from sulfur. This would require further process engineering.

Experimental

For all performed experiments and measurements, the following chemicals were used: bismuth telluride (abcr, 99.99%-Bi), antimony telluride (abcr, 99.999% metals basis), sulfur (Carl Roth, ≥99.5%), tellurium (abcr, 99 999%) and antimony sulfide (Sigma Aldrich, ≤100%).

Chemical vapour transport in closed experimental setups

The respective reagents were mixed using an agate mortar and filled into a quartz ampoule (length: 20 cm, inner diameter: 14.5 mm, outer diameter: 17 mm). The ampoule was sealed at 0.001 mbar. The transport reactions were carried out in a three-zone oven (Carbolite TZF 12/65/550). Heating of the closed experimental setups was performed at a rate of approximately 30 °C min^{-1}. The source of the transport reaction was placed in one of the outer oven zones, and the sink was located in the middle of the oven. During the cool-down process, the source of the ampoules was pulled out of the oven by 1 cm to deposit sulfur in this area.

Different temperature gradients in the range of 300 °C to 425 °C were applied for 72 h. In the case of the Bi_2Te_3/S system, 625 mg (0.780 mmol) of bismuth telluride and 150 mg (4.68 mmol) of sulfur were used, resulting in a Te : S molar ratio of 1 : 2. In the case of the Sb_2Te_3/S system, 488 mg (0.780 mmol) of antimony telluride and 150 mg (4.68 mmol) of sulfur were used. A list of all the experiments carried out can be found in the ESI (Table S1† for the Bi_2Te_3/S system and Table S2† for the Sb_2Te_3/S system).

Three different reaction times (24 h, 48 h and 72 h) and two different Te : S molar ratios (1 : 1.25 and 1 : 2) were applied. For a Te : S molar ratio of 1 : 1.25, 625 mg (0.780 mmol) of bismuth telluride and 94 mg (2.9 mmol) of sulfur were used. For a Te : S molar ratio of 1 : 2, 625 mg (0.780 mmol) of bismuth telluride and 150 mg (4.68 mmol) of sulfur were used. Two different temperature gradients (375 → 325 °C and 425 → 325 °C) were used to investigate the molar ratio between tellurium and sulfur and the reaction time. A list of all the experiments carried out can be found in Table S3 in the ESI.†

Additionally, a set of different reaction times (1 h, 2 h, 4 h, 8 h, 24 h, 48 h, and 72 h) was applied with a temperature gradient of 425 → 325 °C to investigate the recovery rate in closed experimental setups depending on the reaction time. For each ampoule, 625 mg (0.780 mmol) of bismuth telluride and 94 mg (2.9 mmol) of sulfur were used. A list of all the experiments carried out can be found in Table S4 in the ESI.†

Chemical vapour transport in open experimental setups

All recovery processes using the open experimental setup were performed inside a quartz tube (length: 115 cm, inner/outer diameter: 14.5 mm/17 mm or 27 mm/30 mm). The two different tube diameters were used to investigate the scalability of the recovery process. The transport reactions were carried out in a three-zone oven (Carbolite TZF 12/65/550). Additionally, a heating jacket (Horst HMT-900 °C) was used to generate a fourth heating zone. Heating of the open experimental setups was performed at a rate of approximately 30 °C min^{-1}.

For the smaller tube diameter (inner/outer diameter: 14.5 mm/17 mm, cross-sectional area: 1.65 cm^2), 416 mg (0.520 mmol) of bismuth telluride or 326 mg (0.520 mmol) of antimony telluride and 1.50 g (46.8 mmol) of sulfur were mixed using an agate mortar and filled into the quartz tube at the middle of the third heating zone (T_3 in Fig. 7). Additionally, 1.50 g of sulfur (46.8 mmol) was filled into the quartz tube in the middle of the fourth heating zone.

For the larger tube diameter (inner/outer diameter: 27 mm/30 mm, cross-sectional area: 5.73 cm^2), which was used for upscaling investigations, 832 mg (1.04 mmol) of bismuth telluride or 652 mg (1.04 mmol) of antimony telluride and 3.00 g of sulfur (93.6 mmol) were mixed and filled into the quartz tube at the middle of the third heating zone. Additionally, 3.00 g (46.8 mmol) sulfur were filled into the quartz tube at the middle of the fourth heating zone. Due to the higher amount of reagents, it was necessary to create a deepening in the glass tube (depth: 1 cm, length: 2 cm) at the two areas where the educts were placed to prevent the larger amount of melted sulfur from covering large parts of the tube.

In both cases, the recovery process was performed using the following procedure. First, the tube was purged with argon (1.5 NL h^{-1} cm^{-2}) for 15 min to guarantee an inert atmosphere during the reaction. Second, the argon flow was adjusted to the appropriate value (0.15 or 1.5 NL h^{-1} cm^{-2}). Afterwards, the three heating zones of the oven were activated. The respective temperature gradients between 300 °C and 500 °C were held for 1 h. After 0.5 h, the heating jacket was heated to a temperature of 500 °C and held at this temperature for 0.5 h to add a second gas flow of sulfur to the process. The four heating zones were turned off and cooled to room temperature at the end under an argon flow of 0.15 NL h^{-1} cm^{-2}.

Powder X-ray diffraction

The samples were analysed using an X'Pert Pro MPD with Data Collector (ver. 5.4.0.90) software from Malvern PANalytical. An Empyrean Cu LFF X-ray tube (λ(Cu-K$_\alpha$) = 154.06 pm) at 40 kV and 40 mA was used as the X-ray source. The X-ray beam was focused using Soller slits (0.04 rad), a beam mask (10 mm) and a fixed anti-scatter slit (1°). After the beam was focused, diffraction by the sample occurred, which was placed flat on top of a silicon wafer, followed by an angled anti-scatter slit (0.5°), Soller slits (0.04 rad) and a Nickel Beta-filter towards an X'Celerator with a Fass detector. A Bragg-Brentano geometry was used with a PW3050/60 goniometer between 15° and 60° for 2θ at room temperature under an ambient atmosphere. Subsequently, the diffractograms were background corrected using HighScore Plus (ver. 3.0e (3.0.5), Malvern PANalytical) and plotted using OriginPro 2023b (ver. 10.0.5.157, OriginLab).

Energy dispersive X-ray analysis

The elemental composition of the recovered tellurium was quantified using a GeminiSEM 560 from Carl Zeiss and the software AztecLive (ver. 6.1) from Oxford Instruments. Characteristic X-ray emission lines[44] between 0 and 6 keV for tellurium, sulfur, bismuth, oxygen, and carbon were analysed. The samples were focused using the software SMART SEM (ver. 6.08) from Carl Zeiss. Each sample was placed on a sticky carbon pad on top of an aluminium sample holder. The measurement was conducted using a 120 µm aperture and 8 kV acceleration voltage at a working distance of 8.5 mm using a Schottky field emitter as an electron source. The detector used was Ultim®Max from Oxford Instruments. Subsequently, the spectra were background corrected and plotted using OriginPro 2023b (ver. 10.0.5.157, OriginLab).

Raman spectroscopy

Tellurium powder samples were analysed using the Raman microscope Senterra from Bruker. Additionally, sulfur powder was measured as a reference. The spectra were recorded in a wavenumber range of 50–650 cm^{-1} with a 3–5 cm^{-1} resolution using a 532 nm laser excitation source. Additionally, the power of the laser was set to 5 mW, with 60 co-additions and an integration time of 6 s. For the sulfur reference measurement, lower energy was needed, and the laser power was changed to 0.2 mW, the co-additions to 20 and the integration time to 3 s. Generally, the samples were placed on a glass substrate and analysed afterwards. Subsequently, the spectra were background corrected and plotted using OriginPro 2023b (ver. 10.0.5.157, OriginLab).

Thermal analysis

Differential scanning calorimetry. Differential scanning calorimetry of the chemical vapour transport was carried out using a DSC 404 C Pegasus® instrument from NETZSCH. The measurements were performed in quartz ampoules with a flat bottom (length: 1 cm, inner diameter: 4 mm, outer diameter: 6 mm) in a temperature range of 20 °C to 500 °C at a heating rate of 5 K min^{-1} and a constant argon flow of 150 mL min^{-1}. 10–15 mg of the respective sample were used for each ampoule. As reagents, bismuth telluride, antimony telluride, sulfur, tellurium, and antimony sulfide were used. The ampoules were evacuated and refilled with argon three times. Afterwards, they were sealed with an argon pressure of 500 mbar. Finally, the data were analysed using Proteus Thermal Analysis (ver. 6.1.0, NETZSCH) and plotted using OriginPro 2023b (ver. 10.0.5.157, OriginLab).

Simultaneous thermal analysis. The purity of tellurium was assessed *via* simultaneous thermal analysis (differential thermal analysis + thermogravimetry) using an STA 409 PC Luxx® coupled to a QMS 403 Aëolos Quadro mass spectrometer from NETZSCH. Mass spectroscopic signals were recorded using the quasi-multiple ion detection method (QMID). The measurements were performed in Al_2O_3 crucibles in a temperature range of 20 °C to 500 °C at a heating rate of 5 K min^{-1}, a constant synthetic air flow of 30 mL min^{-1} and a protective argon flow of 20 mL min^{-1}. For each measurement, 15–20 mg of the respective sample were used. Subsequently, the data were analysed using Proteus Thermal Analysis (ver. 6.1.0, NETZSCH) and plotted using OriginPro 2023b (ver. 10.0.5.157, OriginLab).

Data availability

The data supporting this article have been included as part of the ESI.†

Conflicts of interest

There are no conflicts to declare.

Acknowledgements

The authors gratefully acknowledge JLU Giessen for a supportive startup financing of this work.

References

1 S. Philipps and W. Warmuth, *Photovoltaics Report*, Fraunhofer Institute for Solar Energy Systems, ISE with support of PSE Projects GmbH, **https://www.ise.fraunhofer.de**, 2023.

2 N. T. Nassar, H. Kim, M. Frenzel, M. S. Moats and S. M. Hayes, *Resour., Conserv. Recycl.*, 2022, **184**, 106434.

3 C. Schuyler Anderson, *Mineral Commodity Summaries* 2022 - *Tellurium*, available at: **https://pubs.usgs.gov/periodicals/mcs2022/mcs2022-tellurium.pdf**, (accessed December 2024).

4 Z. Li, F. Qiu, Q. Tian, X. Yue and T. Zhang, *J. Cleaner Prod.*, 2022, **366**, 132796.

5 O. P. Missen, R. Ram, S. J. Mills, B. Etschmann, F. Reith, J. Shuster, D. J. Smith and J. Brugger, *Earth-Sci. Rev.*, 2020, **204**, 103150.

6 (*a*) K. Hans Wedepohl, *Geochim. Cosmochim. Acta*, 1995, **59**, 1217–1232; (*b*) A. G. Christy, *Mineral. Mag.*, 2015, **79**, 33–49.

7 A. Mahmoudi, S. Shakibania, M. Mokmeli and F. Rashchi, *Metall. Mater. Trans. B*, 2020, **51**, 2555–2575.

8 Z. Xu, Z. Li, D. Li, X. Guo, Y. Yang, Q. Tian and J. Li, *Metals*, 2020, **10**, 1176.

9 M. A. Green, *Sol. Energy Mater. Sol. Cells*, 2013, **119**, 256–260.

10 M. A. Green, *Prog. Photovolt: Res. Appl.*, 2009, **17**, 347–359.

11 (*a*) S. Carrara, S. Bobba, D. Blagoeva, P. Alves Dias, A. Cavalli, K. Georgitzikis, M. Grohol, A. Itul, T. Kuzov, C. Latunussa, L. Lyons, G. Malano, T. Maury, A. Prior Arce, J. Somers, T. Telsnig, C. Veeh, D. Wittmer, C. Black, D. Pennington and M. Christou, *Supply chain analysis and material demand forecast in strategic technologies and sectors in the EU – A foresight study*, Publications Office of the European Union, Luxembourg, 2023; (*b*) Directorate-General for Internal Market, Industry, Entrepreneurship and SMEs, S. Bobba, S. Carrara, J. Huisman, F. Mathiuex and C. Pavel, *Critical Raw Materials for Strategic Technologies and Sectors in the EU - A Foresight Study*, Publications Office of the European Union, Luxembourg, 2020.

12 F.-G. Simon, O. Holm and W. Berger, *Waste Manage.*, 2013, **33**, 942–947.

13 X. Zhang, D. Liu, W. Jiang, W. Xu, P. Deng, J. Deng and B. Yang, *J. Mater. Res. Technol.*, 2020, **9**, 6977–6986.

14 D. Kong, D. Chen, Z. Kuang, C. Xu, B. Feng, X. Hu, Z. Chen, Y. Ma, X. an Fan, G. Li and Y. Li, *Mater. Res. Express*, 2021, **8**, 115901.

15 J. Ma, T. Shi, Y. Li, B. Yang, Y. Tian, B. Xu, H. Yang, X. Chen and C. Chen, *J. Environ. Manage.*, 2023, **327**, 116845.

16 J. Ma, T. Shi, Y. Zhang, D. Huang, Y. Li, B. Yang, Y. Tian, B. Xu, H. Yang, X. Chen and C. Chen, *J. Mater. Res. Technol.*, 2023, **26**, 3003–3014.

17 (*a*) D. J. Bradwell, S. Osswald, W. Wei, S. A. Barriga, G. Ceder and D. R. Sadoway, *J. Am. Chem. Soc.*, 2011, **133**, 19971–19975; (*b*) S. Menezes, *Thin Solid Films*, 2001, **387**, 175–178.

18 G. Sextl, M. Binnewies, A. Bittner, K. Müller-Buschbaum, A. Sedykh, L. H. Bemfert, P. Schmidt and T. Donath, WO/2023/117905, 2022.

19 L. H. Bemfert, J. Burkhart, A. Sedykh, S. Richter, E. Mitura, M. Maxeiner, G. Sextl and K. Müller-Buschbaum, *ChemSusChem*, 2024, e202400785.

20 (*a*) L. Mond, C. Langer and F. Quincke, *J. Chem. Soc., Trans.*, 1890, **57**, 749–753; (*b*) W. C. Roberts-Austen, *Nature*, 1898, **59**, 63–64; (*c*) M. Binnewies, R. Glaum, M. Schmidt and P. Schmidt, *Z. Anorg. Allg. Chem.*, 2013, **639**, 219–229; (*d*) M. Binnewies, *Chem. Unserer Zeit*, 1998, **32**, 15–21; (*e*) A. E. van Arkel and J. H. de Boer, *Z. Anorg. Allg. Chem.*, 1925, **148**, 345–350.

21 M. Binnewies, *Z. Anorg. Allg. Chem.*, 1976, **422**, 43–46.

22 J. Taavitsainen and R. S. Laitinen, *Main Group Chem.*, 1999, **3**, 59–67.

23 (*a*) R. He, G. Schierning and K. Nielsch, *Adv. Mater. Technol.*, 2018, **3**, 1700256; (*b*) G. Tan, M. Ohta and M. G. Kanatzidis, *Philos. Trans. R. Soc., A*, 2019, **377**, 20180450; (*c*) H. J. Goldsmid, *Materials*, 2014, **7**, 2577–2592.

24 (*a*) C. Balarew and M. Ivanova, *Cryst. Res. Technol.*, 1986, **21**, K171–K175; (*b*) H. Schäfer, *Z. Anorg. Allg. Chem.*, 1982, **489**, 154–160; (*c*) H. Schäfer, H. Plautz, C. Balarew and J. Bazelkov, *Z. Anorg. Allg. Chem.*, 1978, **440**, 130–136; (*d*) B. Vengatesan, N. Kanniah and P. Ramasamy, *Mater. Chem. Phys.*, 1987, **17**, 311–316; (*e*) B. Vengatesan, N. Kanniah and P. Ramasamy, *Mater. Sci. Eng., A*, 1988, **104**, 245–247; (*f*) E. H. Carlson, *J. Cryst. Growth*, 1972, **12**, 162–168; (*g*) D. Cubicciotti and F. J. Keneshea, *J. Phys. Chem.*, 1959, **63**, 295–296; (*h*) D. Cubicciotti, *J. Phys. Chem.*, 1961, **65**, 521–523; (*i*) V. Krämer, *Thermochim. Acta*, 1976, **15**, 205–212; (*j*) J. D. Corbett, S. von Winbush and F. C. Albers, *J. Am. Chem. Soc.*, 1957, **79**, 3020–3024; (*k*) M. Schöneich, M. P. Schmidt and P. Schmidt, *Z. Anorg. Allg. Chem.*, 2010, **636**, 1810–1816; (*l*) I. Sommer, *J. Cryst. Growth*, 1972, **12**, 259–260.

25 (*a*) A. Bahrami, G. Schierning and K. Nielsch, *Adv. Energy Mater.*, 2020, **10**, 1904159; (*b*) O. Velázquez-Martinez, A. Kontomichalou, A. Santasalo-Aarnio, M. Reuter, A. J. Karttunen, M. Karppinen and R. Serna-Guerrero, *Resour., Conserv. Recycl.*, 2020, **159**, 104843.

26 (*a*) P. T. Anastas and J. C. Warner, *Green Chemistry*, Oxford University PressOxford, 2000; (*b*) P. Jessop, *Green Chem.*, 2020, **22**, 13–15.

27 B. Meyer, *Chem. Rev.*, 1976, **76**, 367–388.

28 M. Thackray, *J. Chem. Eng. Data*, 1970, **15**, 495–497.

29 F. Fehér, G. P. Görler and H. D. Lutz, *Z. Anorg. Allg. Chem.*, 1971, **382**, 135–148.

30 G. W. Miller, *J. Appl. Polym. Sci.*, 1971, **15**, 1985–1994.

31 A. V. Tobolsky, *J. Polym. Sci., Part C*, 1966, **12**, 71–78.

32 W. M. Haynes, D. R. Lide and T. J. Bruno, *CRC Handbook of Chemistry and Physics*, Taylor & Francis Group, Boca Raton, 2014.

33 F. C. Kracek, *J. Am. Chem. Soc.*, 1941, **63**, 1989–1990.

34 G. Ghosh, *J. Phase Equilib.*, 1994, **15**, 349–360.

35 J.-C. Lin, R. C. Sharma and Y. A. Chang, *J. Phase Equilib.*, 1996, **17**, 132–139.

36 F. M. Jaeger and H. S. van Klooster, *Z. Anorg. Chem.*, 1912, **78**, 245–268.

37 C. Adenis, V. Langer and O. Lindqvist, *Acta Crystallogr., Sect. C:Cryst. Struct. Commun.*, 1989, **45**, 941–942.

38 B. E. Warren and J. T. Burwell, *J. Chem. Phys.*, 1935, **3**, 6–8.

39 A. Kyono and M. Kimata, *Am. Mineral.*, 2004, **89**, 932–940.

40 W. Hofmann, *Z. Kristallogr. – Cryst. Mater.*, 1933, **86**, 225–245.

41 (*a*) A. S. Pine and G. Dresselhaus, *Phys. Rev. B*, 1971, **4**, 356–371; (*b*) J.-W. Liu, F. Chen, M. Zhang, H. Qi, C.-L. Zhang and S.-H. Yu, *Langmuir*, 2010, **26**, 11372–11377; (*c*) M. Safdar, X. Zhan, M. Niu, M. Mirza, Q. Zhao, Z. Wang, J. Zhang, L. Sun and J. He, *Nanotechnology*, 2013, **24**, 185705; (*d*) J. U. Salmón-Gamboa, A. H. Barajas-Aguilar, L. I. Ruiz-Ortega, A. M. Garay-Tapia and S. J. Jiménez-Sandoval, *Sci. Rep.*, 2018, **8**, 8093; (*e*) J.-M. Song, Y.-Z. Lin, Y.-J. Zhan, Y.-C. Tian, G. Liu and S.-H. Yu, *Cryst. Growth Des.*, 2008, **8**, 1902–1908; (*f*) B. H. Torrie, *Solid State Commun.*, 1970, **8**, 1899–1901.

42 R. R. Silva, H. A. G. Mejia, S. J. L. Ribeiro, L. K. Shrestha, K. Ariga, O. N. Oliveira, Jr., V. R. Camargo, L. J. Q. Maia and C. B. Araújo, *J. Braz. Chem. Soc.*, 2017, **28**, 58–67.

43 S. Khatun, A. Banerjee and A. J. Pal, *Nanoscale*, 2019, **11**, 3591–3598.

44 J. A. Bearden, *Rev. Mod. Phys.*, 1967, **39**, 78–124.